13kV UHV-IGBT: Feasibility Study

Atsushi Ito and Ichiro Omura
Kyushu Institute of Technology, Kitakyushu, Japan,
atsushi.ito262@mail.kyutech.jp, omura@ele.kyutech.ac.jp

***Abstract*—Increasing the rated voltage of IGBTs is indispensable for realizing future energy transmission systems such as gigawatt-class UHVDC and high-power motor drives with reduced number of series connection or simplified circuit topology. The voltage of IGBTs, however, has stagnated for 20 years at 6.5kV because of several issues. In this paper, we investigated the feasibility of a 13kV ultra-high voltage IGBT with twice the breakdown voltage of conventional IGBTs using TCAD simulations. As a result, the use of a double gate structure proved to be practical under DC bus voltage of 6.6 kV and a switching frequency of 150 Hz.**

Keywords—13kV Si IGBT, UHV IGBT, Double gate, TCAD simulations

I. INTRODUCTION

Renewable energies such as wind power and hydroelectric power are often located far away from large consumption areas, and their output is unstable, requiring wide-area coordination by power grid with long-distance transmission. It is expected to increase demand for high-voltage applications such as gigawatt-class UHV(Ultra High Voltage) DC transmission. The development of UHV-IGBT is essential for these future energy transmission systems. Also, it is expected that UHV-IGBTs will bridge to next generation SiC devices which need little more time for practical use in high power application.

Increasing the withstand voltage of Si-IGBT exceeding 6.5kV has not been studied for about 20 years due to several reasons, such as requirement of extremely thick wafer, fabrication process with maintaining crystal quality, heat dissipation with elevated heat density and package technology for higher voltage [1-3].

In this study, a feasibility study of 13kV-Si-IGBT for single -side gate and double-side gate structures was carried out with TCAD simulation focusing to conduction losses and switching losses and discuss about possible switching frequency under 6.6kV DC-link voltage operations.

II. DEVICE DESIGN OF 13 KV UHV-IGBT

A. N-base Design

N-base is designed considering the following points.

-- Minimize N-base length to reduce the conduction losses under maintain 15 kV at room temperature.

-- Set carrier lifetime in N-base with sufficient carrier diffusion length to the long N-base.

-- Cosmic-ray induced single event burnout (SEB) failure rate assessment with Zeller's formula [4].

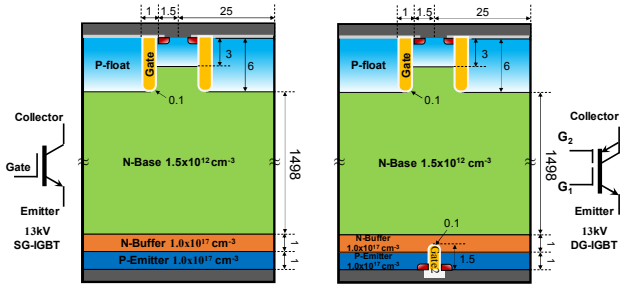

Fig. 1 13kV SG-IGBT structure and 13kV DG-IGBT structure (Drive voltage 15V for both gates)

B. MOS gate structure design

Trench IGBT structure with mesa width of 3μm and trench depth of 6μm. Cell width is as large as 50μm to increase electron injection efficiency with injection enhancement (IE-) effect ([1] ,[5]) since reducing voltage drop across the N-base with high level carrier storage is more important than MOS channel resistance reduction for minimized conduction loss of UHV-IGBTs.

A double gate structure with back-side gate is studied, as well as the single gate IGBT, for expected reduced turn-off losses [6-10]. The selected back side gate structure is, so called, MOS controlled thyristor (MCT) type [11]. MCT-type back side gate has integrated N-MOS transistor to bypass electron current during turn-off so that hole injection from P-emitter is suppressed and thus the tail current will be dramatically reduced. MCT-type back-side gate has several advantage over the other back-side gate structures such as emitter switched thyristor type (EST-type) [12]. (1) Integrated N-MOS channel resistance does not affect conduction voltage Vce(sat), (2) Electron mobility advantage for the integrated N-MOS channel, (3) No anode short effect of N-buffer layer exists. While, EST-type structure has disadvantage of series P-MOS channel resistance effect in Vce(sat) and the strong anode short effect to N-buffer layer with N-well contact to collector electrode.

III. SIMULATION RRESULTS AND DISCUSSIONS

A. Static Characteristics

The simulated UHV-IGBT structure has a device thickness of 1500 μm and an N-based donor concentration (N_D) of 1.5×10^{12} cm^{-3} as shown as Fig.1. Both single gate (SG) structure and double gate (DG) structure are prepared for the simulations. The simulated SG-IGBT and the DG-IGBT has identical characteristics under static operation with breakdown voltage of 17 kV and about 3.0 V of Vce(sat) at 25 A/cm^2 collector current as shown Fig. 2 and Fig. 3.

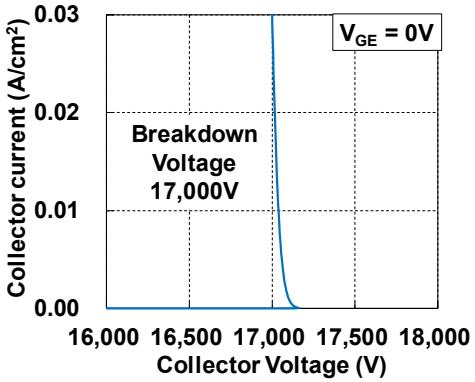

Fig. 2 Simulated reverse bias characteristics of 13kV UHV-IGBT. (SG-IGBT and DG-IGBT have identical characteristics)

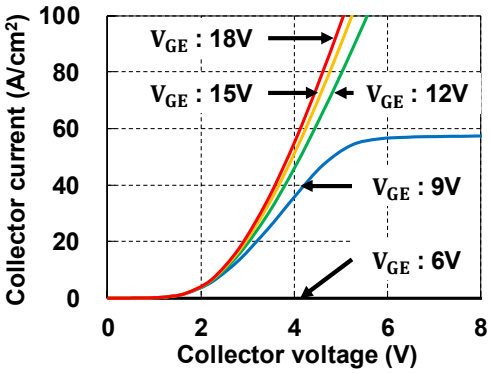

Fig. 3 Simulated forward conduction characteristics (under back-side gate voltage of 0V for DG-IGBT).

B. Resistive Load Switching of UHV-IGBT

Resistive load switching simulation circuit is shown in Fig.4. Front-side gate G_1 and back-side gate G_2 are driven simultaneously for DG-IGBT. Figure 5 compares stored carrier distributions in the N-base for time steps during turn-off transient for SG-IGBT and DG-IGBT. Thanks to the back gate structure, the stored carriers in N-base were swept out from both emitter-side and collector-side, and which enhanced the turn-off speed. Total switching loss (E_{SW}) and Vce(sat) trade-offs for SG- and DG-IGBT is shown in Fig. 6. The curves are obtained by varying P-emitter injection efficiency. 30 % switching loss reduction with double gate structure is observed.

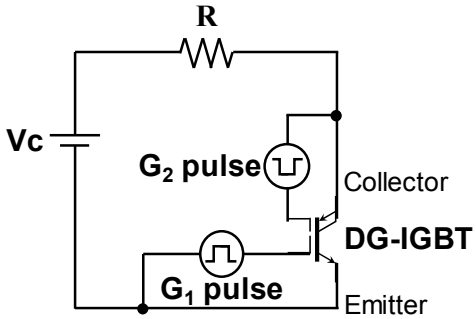

Fig. 4 Resistive load switching circuit for TCAD simulation. Front side gate and back-side gate are driven in the same timing

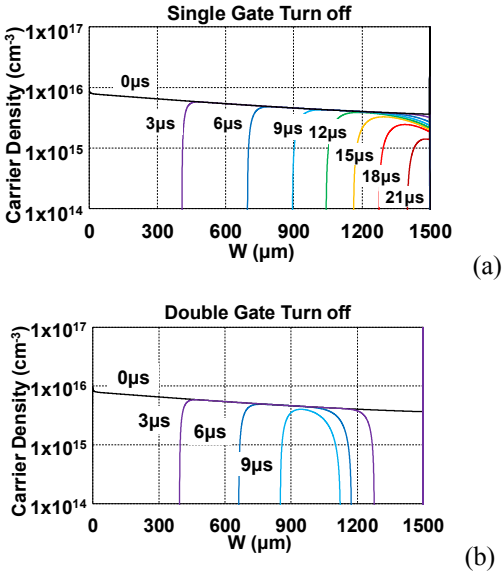

Fig. 5 Comparison of carrier distribute between 13kV SG-IGBT (a) and 13kV DG-IGBT (b).

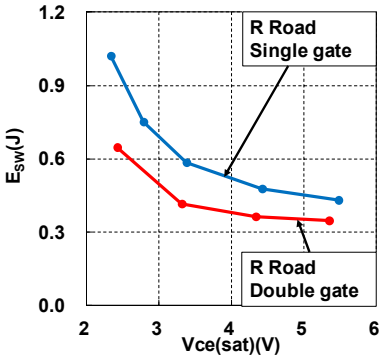

Fig. 6 Vce(sat) - E_{SW} trade-off curve under resistive load for 13kV UHV-IGBT. G_1 and G_2 timing difference is set to 0 µsec.

C. Inductive Load Switching of UHV-IGBT

13kV UHV-PiN Diode was designed on TCAD for the use in inductive load switching simulations. The PiN diode has identical i-layer structure with the IGBT and has shallow P- and N-emitter to reduce reverse recovery charge. Circuit inductance L_S was taken into account in the switching simulations as shown in Fig.7. Fig.8 show the turn-on and turn-off waveforms example of the DG-IGBT. The gate timing difference between G_1 and G_2 was set to be 0 us for the simulations for simplicity. Reduced stray inductance causes large PiN diode reverse recovery current (Fig. 8 (b)) due to long i-layer and large stored carrier charge, while with large L_S, diode reverser recovery current has reduced (Fig. 8 (a)) and which is effective for reducing turn-on loss of UHV-IGBT. This implies that current snubber circuit to reduce dI/dt during turn-on can be effective to reduce switching loss.

Turn-off waveforms in Fig.8 (c) and (d) shows terrace and abrupt drop in collector current because of the carrier swept out from both side of the N-base, i.e. when the depletion layers from top side and bottom side of N-base meet each other (see Fig. 5 (b)) there remains no storage carrier to maintain the tail current. This may cause collector voltage spike. So, voltage

clumping snubber circuit with sufficiently low stray inductance is needed for practical application of UHV-IGBTs.

Trade off curves between total switching loss (sum of turn-on loss and turn-off loss of IGBT) and Vce(sat) for L_S are shown in Fig. 9. Table. 1 shows total loss of UHV-IGBT under 6.6 kV DC link voltage at switching frequency of 50 Hz and 150 Hz at room temperature. The values are calculated from the trade-off curve shown in Fig. 9. Total loss consists of conduction loss, turn-on loss and turn-off loss.

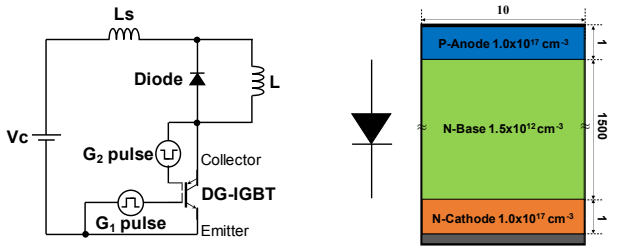

Fig. 7 Inductive load switching circuit for TCAD simulation with 13kV UHV-PiN diode model.

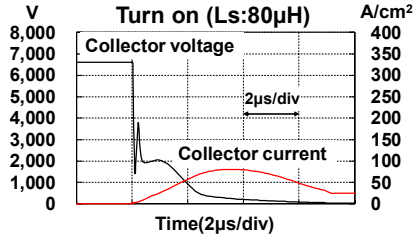

(a)

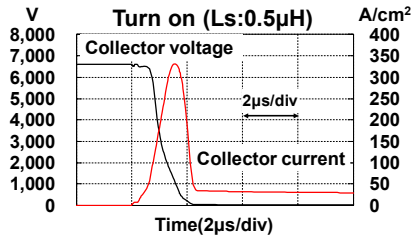

(b)

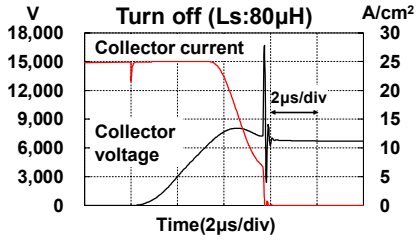

(c)

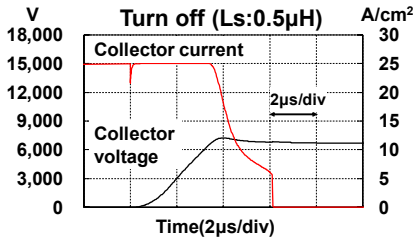

(d)

Fig. 8 13kV DG-IGBT inductive load switching waveform for (a)turn-on (L_S=80 μH), (b) turn-on (L_S=0.5 μH), (c) turn-off (L_S=80 μH), (d) turn-off(LS=0.5 μH).

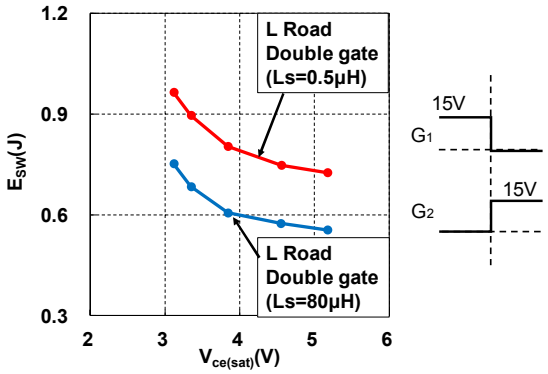

Fig. 9 Vce(sat) - E_{SW} trade-off curve under inductive load for 13kV UHV-IGBT. G_1 and G_2 timing difference is set to 0 μsec.

Table. 1 Total loss (=heat generation) of UHV-IGBT under 6.6 kV DC link voltage at switching frequency of 50 Hz and 150 Hz at room temperature, calculated from Fig. 9.

V_{DC}	6600 V	
I	25 A/cm²	
f_{SW}	50 Hz	150 Hz
Total loss (Ls:0.5μH)	87 W/cm²	169 W/cm²
Total loss (Ls:80μH)	76 W/cm²	139 W/cm²

D. Application Examples of 13 kV UHV-IGBTs

According to the result shown in Table 1, 13kV UHV-IGBTs are suitable for Modular Multilevel Converters (MMCs), which is used in HVDC system, with advantages of low conduction losses than series of 4.5-6.5kV IGBTs [13]. Further, HVDC breakers are also suitable application to half the number of series connection [14]. As an another possibility, 13kV UHV IGBTs will expand the application of three-level neutral-point clumped (NPC) inverters ([15]) to 6.6 kV motor drive with 150 Hz switching performance and 6.6 kV NPC has advantage in simplified system, high efficiency and smaller volume than Robicon type converters ([16]).

E. Drive Timing Optimization for Back-Side Gate

Influence of gate drive timing difference between G_1 and G_2 on to turn-off loss is investigated [6]. Figure 10 shows turn-off loss as a function of gate time difference ΔT_{Gate}. Simultaneous timing for both gates (ΔT_{Gate}=0s) sufficiently reduce turn-off loss. For turn-on, gate G_2 should be under off-biased before G_1 biased to turn-on the DG-UHV-IGBT.

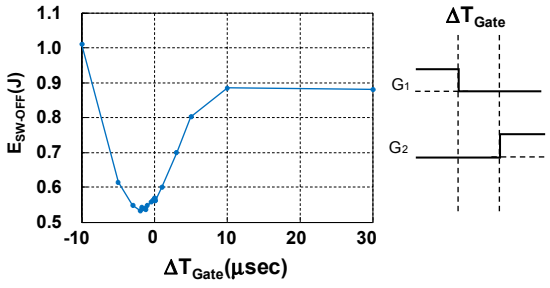

Fig. 10 Optimization of gate trigger time difference for turn-off between two gates G_1 and G_2.(L_S=0 μH).

F. Edge Termination

The edge termination with guard ring structure successfully withstands 15 kV with a termination length of 5000μm as shown in Fig.11 and Fig.12.

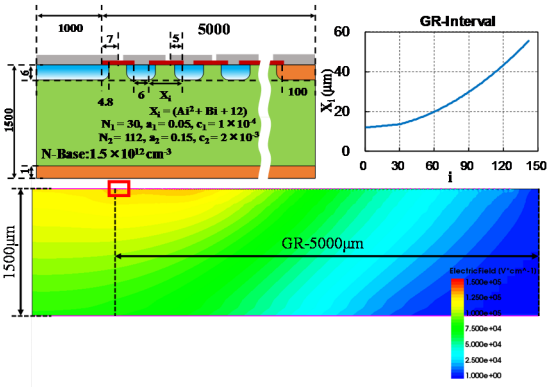

Fig. 11 Edge termination structure with 142 guard rings, guard ring interval design (window-window distance for i-th and i+1 guard-rings) and electric field in termination area

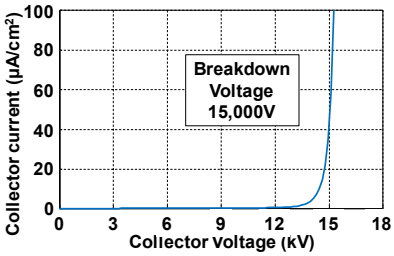

Fig. 12 TCAD obtained breakdown voltage of termination structure with 142 guard rings.

G. Carrier Lifetime Requirements

The required lifetime can be calculated by the ambipolar diffusion length.

$$L_A = \sqrt{\frac{kT}{q}\frac{2\mu_p\mu_n}{\mu_p+\mu_n}\tau}$$

The carrier lifetime in N-base of UHV-IGBT is 1.28ms ($\tau = \tau_p + \tau_n$) for simulation. The carrier lifetime required for IGBTs can be calculated by the condition of $L_A \cong N\ base\ length$, as shown in Fig.13, and it can be seen that UHV-IGBTs need very long carrier lifetime after the fabrication process.

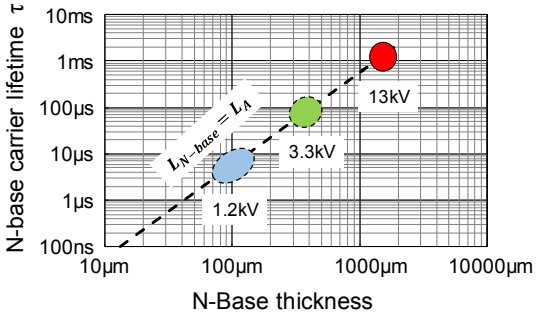

Fig. 13 Required carrier lifetime for N-base after the fabrication process.

IV. CONCLUSION

13kV UHV-IGBT can achieve total power loss of 76W/cm^2 under the operation condition of DC link voltage 6.6kV with switching frequency of 50 Hz and 139W/cm^2 at 150Hz at room temperature. Double gate structure is effective to reduce the losses. Edge termination design and carrier lifetime requirements are also discussed.

UHV-IGBTs are suitable for MMCs and HVDC breakers to half the number of series connection. UHV-DG-IGBTs will expand the application of three-level NPC inverters to 6.6 kV motor drive with 150 Hz switching performance.

According to the simulation results and discussions, it is worth to consider demonstrative researches of UHV-IGBT, from chip, wafer, package and power electronics application view point.

REFERENCES

[1] M. Kitagawa, I. Omura, S. Hasegawa, T. Inoue and A. Nakagawa, "A 4500 V injection enhanced insulated gate bipolar transistor (IEGT) operating in a mode similar to a thyristor", Proc. IEEE IEDM, pp. 679-682, 1993.

[2] T. Wikstrom, F. Bauer, S. Linder and W. Fichtner, "Experimental study on plasma engineering in 6500V IGBTs", Proc. ISPSD '00, 2000.

[3] K. Hatori, Y. Sakai, S. Kitamura, T. Motomiya, K. Ota, Y. Kitajima, S. Iura, H. Yamaguchi, and K. Kurachi, "Experimental study on plasma engineering in 6500 V IGBTs", IEEE ECCE, pp.2897-2900, 2014.

[4] H. R. Zeller, "Cosmic Ray Induced Failures in High Power Semiconductor Devices," Solid-State Elec. 38, pp. 2041-2046, 1995.

[5] I. Omura, T. Ogura, K. Sugiyama and H. Ohashi "Carrier injection enhancement effect of high voltage MOS devices-device physics and design concept" Proc. of ISPSD '97, 1997.

[6] T. Ogura, A. Nakagawa, K. Takigami, M. Atuta, and Y. Kamei, "High frequency 6000 V double gate GTOs", Technical Digest., IEDM, 1988.

[7] K. D. Hobart, F. J.Kub, G. Dolny, M. Zafrani, J. M. Neilson, J. Gladish, and C. McLachlan, "A fabrication of a double-side IGBT by very low temperature wafer bonding", Proc. of ISPSD '99, pp.45-48, 1999.

[8] M. Baus, B.N. Szafranek, St. Chemielus, B. Hadam, B. Spangenberg, R. Sittig, and H. Kurz, "Fabrication of Monolithic Bidirectional Switch (MBS) devices with MOS-controlled emitter structures", Proc. of ISPSD '06, PP.181-184, 2006.

[9] A. Bourennane, H. Tahir, J-L. Sanchez, L. Pont, G. sarrabayrouse, and E. Imbernon, "High temperature wafer bonding technique for the realization of a voltage and current bidirectional IGBT", Proc. of ISPSD '11, pp.140-143, 2011.

[10] Shohei Harada, "Double Sided Gate IGBT and Optimal Gate Control Method," CIPS, 2016.

[11] V. A. K. Temple, "Semiconductor device having turn-on and turn-off capabilities." US Patent, US4816892A, 1987.

[12] M. S. Shekar, M. Nandakumar, B. J. Baliga, "Unit cell arrangement for emitter switched thyristor with base resistance control," US Patent, US5294816A, 1992.

[13] Toshiba Energy Systems & Solutions Corporation, "New Hokkaido-Honshu VSC HVDC Commissioned, Interconnecting Hokkaido and the Main Island of Honshu," https://www.toshiba-energy.com, 2019.

[14] C. M. Franck, "HVDC Circuit Breakers: A Review Identifying Future Research Needs," in IEEE Trans. on Power Delivery, 26, 2, pp. 998-1007, 2011.

[15] A. Nabae, I. Takahashi and H. Akagi, "A New Neutral-Point-Clamped PWM Inverter," in IEEE Trans. on IA, 17, 5, pp. 518-523, Sept. 1981.

[16] P. W. Hammond, "Medium voltage PWM drive and method," US Patent, US5625545A, 1994.